Journal of Hydraulic Research

ISSN: 0022-1686 (Print) 1814-2079 (Online) Journal homepage: www.tandfonline.com/journals/tjhr20

Pier scour in clear water for sediment mixtures

Junke Guo

To cite this article: Junke Guo (2012) Pier scour in clear water for sediment mixtures, Journal of Hydraulic Research, 50:1, 18-27, DOI: 10.1080/00221686.2011.644418

To link to this article: https://doi.org/10.1080/00221686.2011.644418

Published online: 12 Jan 2012.

Journal of Hydraulic Research Vol. 50, No. 1 (2012), pp. 18–27
http://dx.doi.org/10.1080/00221686.2011.644418

Research paper

Pier scour in clear water for sediment mixtures

JUNKE GUO (IAHR Member), *Department of Civil Engineering, University of Nebraska-Lincoln, 1110 S 67th Street, Omaha, NE 68182, USA.*
Email: jguo2@unl.edu

ABSTRACT
The current pier scour design in the USA is mainly based on the CSU equation, yet a recent incisive evaluation indicates a need to change it because substantial advances were made in the last two decades for understanding the pier scour processes. The objective of this research is then to propose a simplified scour mechanism and a physically-based scour depth equation for practical design purposes. A critical review on selected previous studies is first made to form the basis of this research. A simplified scour mechanism is next proposed in terms of the pressure gradient through flow–structure, flow–sediment and sediment–structure interactions. A hypothesis on the equilibrium scour depth equation is then proposed based on the understanding of the scour mechanism and tested by flume data. Finally, the proposed scour depth equation provides a criterion and a rule of thumb for scour design and evaluation.

Keywords: Bridge scour, CSU equation, Hager number, pier scour, sediment mixture

1 Introduction

Bridge scour is an important engineering concern for the US Federal Highway Administration because it is responsible for 60% of river bridge failures (Shirole and Holt 1991). The current pier scour design in the USA is mainly based on the CSU equation described in HEC-18 (Richardson and Davis 2001). Yet, a recent incisive evaluation of bridge scour research (Ettema *et al.* 2011) indicates a need to change it because substantial advances have been made since 1990 in understanding pier scour processes, which should be incorporated into design methods.

This research focuses on clear-water scour at singular circular piers in non-cohesive sediment mixtures. The objective is to provide a new pier scour equation based on the understanding of flow–structure–sediment interactions. Selected previous studies are first reviewed; a simplified scour mechanism is next emphasized in terms of the pressure gradient; a hypothesis on the equilibrium scour depth equation is then developed based on the scour mechanism and tested by flume data. The proposed equation is finally applied for bridge maintenance and design.

2 Literature review

Bridge pier scour has been studied for more than six decades (Inglis 1949) but remains an unsolved problem (Ettema *et al.* 2011) because it is influenced by many flow–structure–sediment factors, particularly the complicated vortex and turbulence structures around piers. Since several reviews on the topic are available (Sumer 2007, Tafarojnoruz *et al.* 2010, Ettema *et al.* 2011, Sheppard *et al.* 2011), this review focuses only on Laursen (1958, 1963), Richardson and Davis (1995, 2001), Melville and Chiew (1999), Oliveto and Hager (2002, 2005) and Sheppard *et al.* (2011), forming the basis of this research.

2.1 *Laursen's equation*

Given a pier in a flume under certain flow and sediment conditions, Laursen (1958) observed that the equilibrium scour depth mainly increases with the approach flow depth. Considering various pier diameters and sediment sizes, Laursen (1963) proposed the relationship

$$\frac{b}{y_s} = 5.5\left[\frac{(y_s/11.5h+1)^{7/6}}{\sqrt{\tau_1/\tau_c}} - 1\right] \tag{1}$$

This means that the scour depth y_s depends on variables of the flow (h, τ_1) with h = approach flow depth and τ_1 = grain bed shear, the pier (b) with b = pier diameter, and the sediment (τ_c) with τ_c = critical shear at sediment threshold. For the maximum potential scour depth y_s at $\tau_1 = \tau_c$, Eq. (1) becomes for

Revision received 23 November 2011/Open for discussion until 31 August 2012.

ISSN 0022-1686 print/ISSN 1814-2079 online
http://www.tandfonline.com

typically $y_s \ll 11.5h$

$$\frac{b}{y_s} = 5.5\left[\left(\frac{y_s}{11.5h}+1\right)^{7/6} - 1\right] \tag{2}$$

Equation (2) is approximated by Ettema *et al.* (2011) as

$$\frac{y_s}{\sqrt{bh}} \approx 1.34 \tag{3}$$

indicating that $(bh)^{1/2}$ is the appropriate scaling length for the pier scour depth.

2.2 *CSU equation*

The widely used CSU equation resulted from a series of studies (Shen *et al.* 1966, Richardson and Davis 1995, 2001, Molinas 2001) at Colorado State University. It determines pier scour as

$$\frac{y_s}{b} = 2K_1K_2K_3K_4\left(\frac{h}{b}\right)^{0.35}\mathsf{F}^{0.43} \tag{4}$$

where $\mathsf{F} = V/(gh)^{1/2}$ approach flow Froude number with V = approach flow velocity and g = gravitational acceleration, K_1 = correction of pier shape ($K_1 = 1$ for circular pier), K_2 = correction of approach flow attack angle ($K_2 = 1$ for regular approach flow), K_3 = correction of bedform ($K_3 = 1$ for clear-water with flat bed) and K_4 = correction of sediment mixtures (K_4 = for uniform sediment). For circular piers in clear-water and sediment mixtures, Eq. (4) becomes

$$\frac{y_s}{b^{0.65}h^{0.35}} = 2K_4\mathsf{F}^{0.43} \tag{5}$$

This means that (i) the scaling length for y_s is $b^{0.65}h^{0.35}$, similar to Eq. (3); (ii) y_s increases with F; and (iii) y_s decreases with increasing sediment non-uniformity $\sigma = (D_{84}/D_{16})^{1/2}$ through K_4. Note that Eq. (5) is independent of sediment size D_{50} at least for uniform sediment.

Although Eq. (4) or (5) provide reasonable scour depths for narrow and intermediate piers (Ettema *et al.* 2011), the use of F is physically unreasonable if h is not very small, because it describes the gravity effect at the free water surface while scour is a phenomenon of water–sediment interactions at the bed. Furthermore, the lack of D_{50} is physically unreasonable because sediment size is the main parameter to limit scour in flow–bed interaction processes, particularly for sediment mixtures. The determination of K_4 as proposed by Molinas (2001) also lacks a clear physical base.

2.3 *Melville–Chiew's equation*

Based on experiments at the University of Auckland and the Nanyang Technological University, Melville and Chiew (1999) stated that (i) pier scour is divided into three categories: narrow, intermediate and wide piers; the maximum potential scour depth y_s is scaled by different lengths as (Kandasamy and Melville 1998)

$$y_s \propto \begin{cases} b & \text{for narrow piers} \\ \sqrt{bh} & \text{for intermediate piers} \\ h & \text{for wide piers} \end{cases} \tag{6}$$

of which the intermediate pier scour is similar to Eq. (3); (ii) for clear-water scour, y_s is almost proportional to V/V_c with V_c = critical approach flow velocity at sediment threshold; and (iii) y_s decreases as sediment coarseness D_{50}/b increases, but y_s is independent of sediment size if $D_{50}/b \leq 0.02$ (fine sands). Note that the definition of the sediment coarseness here is different from b/D_{50} by Melville and Chiew (1999), which is smaller for coarser sands but larger for finer sands.

2.4 *Oliveto–Hager's equation*

This equation resulted from a series of studies (Hager and Oliveto 2002, Oliveto and Hager 2002, 2005) at VAW, Switzerland, improved by Kothyari *et al.* (2007) and Hager and Unger (2010). Hager and Oliveto (2002) stated that the flow–sediment interaction is described by the densimetric particle Froude number

$$\mathsf{H} = \frac{V}{\sqrt{(\rho_s/\rho - 1)gD_{50}}} \tag{7}$$

representing the effect of reduced gravity $(\rho_s/\rho - 1)g$ on the water–sediment interface, similar to the classic Froude number representing the gravity effect on water–air interfaces. This research calls H the Hager number and reserves the densimetric Froude number for continuum densimetric flows where the flow depth instead of sediment size is used. Oliveto and Hager (2002, 2005) obtained the relationship

$$\frac{y_s(t)}{b^{2/3}h^{1/3}} = 0.068K_1\frac{\mathsf{H}^{3/2}}{\sqrt{\sigma}}\log\frac{t\sqrt{(\rho_s/\rho - 1)gD_{50}}}{b^{2/3}h^{1/3}} \tag{8}$$

with $y_s(t)$ as scour depth at time t. Equation (8) does not tend to an equilibrium scour depth at $t = \infty$, but it is expected that the equilibrium scour depth for circular piers has the form

$$\frac{y_s}{b^{2/3}h^{1/3}} \propto \frac{\mathsf{H}^{3/2}}{\sqrt{\sigma}} \tag{9}$$

of which the left-hand side is similar to Eqs. (3) and (5), indicating that y_s is scaled by $b^{2/3}h^{1/3}$. Besides, Eq. (9) states that y_s increases with H but decreases with σ. Equation (8) was improved by Kothyari *et al.* (2007) considering the critical Hager number at sediment threshold, and by Hager and Unger (2010) extending it to unsteady flow scour.

2.5 *Sheppard–Melville's equation*

Ettema *et al.* (2011) recommended replacing the CSU equation with that of Sheppard–Melville, an integration of Sheppard and Miller (2006) and Melville (1997). For clear-water scour, the Sheppard–Melville equation reads (Sheppard *et al.* 2011)

$$\frac{y_s}{b} = 2.5 \mathrm{f}_1 \mathrm{f}_2 \mathrm{f}_3 \tag{10}$$

where the function $\mathrm{f}_1 = \mathrm{f}_1(h/b)$ represents the flow–structure interaction, $\mathrm{f}_2 = \mathrm{f}_2(V/V_c)$ the flow–sediment interaction and $\mathrm{f}_3 = \mathrm{f}_3(D_{50}/b)$ the sediment–structure interaction. For the maximum potential scour depth, Eq. (10) reduces to (Ettema *et al.* 2011)

$$\frac{y_s}{b} = 2.5 \tanh\left[\left(\frac{h}{b}\right)^{0.4}\right] \tag{11}$$

which for shallow water or wide piers $h/b \leq 0.3$ is equivalent to

$$\frac{y_s}{b^{0.6} h^{0.4}} = 2.5 \tag{12}$$

whereas for deep water or narrow piers $h/b \geq 10$

$$\frac{y_s}{b} = 2.5 \tag{13}$$

Equation (10) adds the sediment–structure interaction $\mathrm{f}_3(D_{50}/b)$ to bridge scour, yet neglecting the armoring effect due to σ.

2.6 *Summary*

The above review is summarized as: (i) Pier scour results from flow–structure–sediment interactions. (ii) The flow–structure interaction (h, b) primarily dominates the scour depth as

$$y_s \propto b^{\lambda} h^{1-\lambda} \tag{14}$$

where $0 \leq \lambda \leq 1$. (iii) The flow–sediment interaction (τ_1/τ_c, H with σ, or V/V_c) is the secondary factor governing the scour depth. Since τ_1/τ_c and V/V_c are converted to H through the Shields diagram and a resistance equation (Hager and Oliveto 2002), H with σ is used here to represent the flow–sediment interaction, so that

$$y_s \propto \mathrm{f}(\mathsf{H}, \sigma) \tag{15}$$

(iv) The tertiary factor is the sediment–structure interaction (D_{50}/b), so that y_s is described by

$$\frac{y_s}{b^{\lambda} h^{1-\lambda}} = \mathrm{f}\left(\mathsf{H}, \sigma, \frac{D_{50}}{b}\right) \tag{16}$$

whose specific form is determined based on the understanding of the scour mechanism. Equation (16) is an induction from leading empirical equations in the literature; it is not derived from dimensional analysis so that y_s and D_{50} are not necessarily scaled by the same length scale.

3 Scour mechanism

The scour mechanism was studied by Ettema (1980), Dargahi (1989, 1990), Roulund *et al.* (2005), Dey and Raikar (2007), Unger and Hager (2007), Kirkil *et al.* (2008, 2009) and Veerappadevaru *et al.* (2011). Since the pressure gradient is responsible for all flow and scour phenomena (including the bed-shear stress) around piers, this section qualitatively explains the scour mechanism in terms of pressure gradient through the (i) flow–structure, (ii) flow–sediment and (iii) sediment–structure interactions.

3.1 *Flow–structure interaction*

The flow interacts with a pier in three ways: a vertical stagnation flow divided into up-flow and down-flow on the leading pier face (Fig. 1a), two boundary layers along the upstream pier perimeter (Fig. 1b) and wake flow behind the pier (Fig. 1b).

Assuming that the boundary layer flows of Fig. 1(b) are fully-developed, the pressure is then approximated by Bernoulli's equation according to Prandtl's boundary layer theory

$$\gamma y + p + \frac{1}{2}\rho(u_r^2 + u_\phi^2) = \text{const} \tag{17}$$

where γ = specific water weight, y = distance from bed (Fig. 1a), p = pressure and u_r and u_ϕ (Fig. 1b) = potential

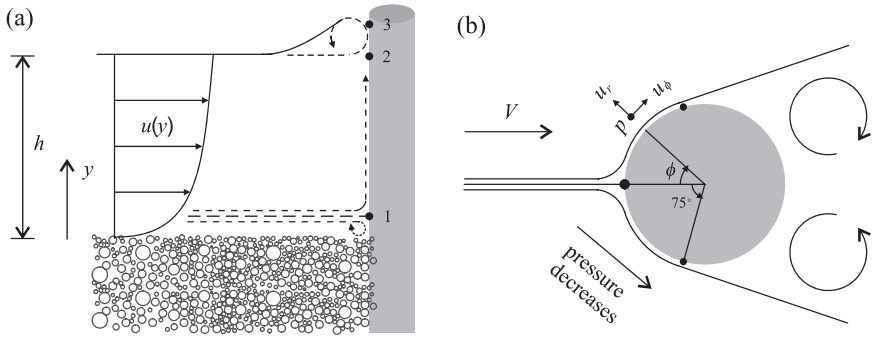

Figure 1 Flow–structure interaction in initial scour phase: (a) side view and (b) plan view

velocities given in cylindrical coordinates by (Julien 2010)

$$u_r = -u(y)\left(1 - \frac{R^2}{r^2}\right)\cos\phi \tag{18}$$

$$u_\phi = u(y)\left(1 + \frac{R^2}{r^2}\right)\sin\phi \tag{19}$$

where $u(y)$ = approach flow velocity at y, ϕ = angle from the leading edge, $R = b/2$ pier radius, and $r \geq R$ distance from the pier centre. Inserting Eqs. (18) and (19) into Eq. (17) gives

$$\gamma y + p + \frac{1}{2}\rho u^2\left(\frac{R^4}{r^4} - 2\frac{R^2}{r^2}\cos 2\phi + 1\right) = \text{const} \tag{20}$$

so that the pressure gradient in the ϕ-direction is

$$\frac{\partial p}{\partial \phi} = -2\rho u^2\left(\frac{R^2}{r^2}\right)\sin 2\phi \tag{21}$$

indicating $\partial p/\partial\phi \leq 0$ for $0 \leq \phi \leq 90°$, or the flow–structure interaction results in a favourable pressure gradient in the ϕ-direction upstream of the pier (Fig. 1b). Note that a theoretical bed elevation (Einstein and El-Samni 1949), below roughness surface, is applied for rough walls if Eq. (21) is applied, so that $u \neq 0$ at a real bed surface.

Equation (21) describes scour initiation and bed shear around piers: (i) the pressure gradient is zero at the stagnation point ($\phi = 0$, $r = R$), so that no sediment moves downstream from the leading edge at scour start if the asymmetrical shape of natural sediment is neglected; and (ii) the maximum pressure gradient occurs at ($\phi = 45°$, $r = R$), so that scour begins at the upstream pier sides. This analysis qualitatively agrees with literature data. Hjorth (1975) observed that the maximum bed-shear stress occurs at $\phi = 45°$, corresponding to the maximum pressure gradient if momentum conservation is considered. Dargahi (1990) noted that 'the scouring commences after 25 s … at either side of the cylinder at about ±45°'. Roulund *et al.* (2005) calculated the maximum bed-shear stress at $\phi = 45°$–$70°$. Further tests (Unger and Hager 2007) and numerical simulations (Abdelaziz *et al.* 2011) demonstrated that scour starts at $\phi = 75°$ from laminar separation points (White 1991) where vortex shedding forms a wake flow region.

The wake flow, filled with vortices, is described by conservation of vorticity as (Kundu 1990)

$$\frac{\mathrm{D}\boldsymbol{\Omega}}{\mathrm{D}t} = (\boldsymbol{\Omega}\cdot\boldsymbol{\nabla})\mathbf{u} + \nu\nabla^2\boldsymbol{\Omega} \tag{22}$$

where $\mathrm{D}/\mathrm{D}t$ = material derivative, $\boldsymbol{\Omega}$ = vorticity, $\mathbf{u}$ = vector velocity and ν = kinematic water viscosity. The first term of the right-hand side represents the rate of change of vorticity due to stretching and tilting of vortex lines (or tubes), whereas the second term represents the rate of change due to diffusion of vorticity. Referring to Fig. 2 and according to Eq. (22), after parent vortices are created by vortex shedding, velocity gradients

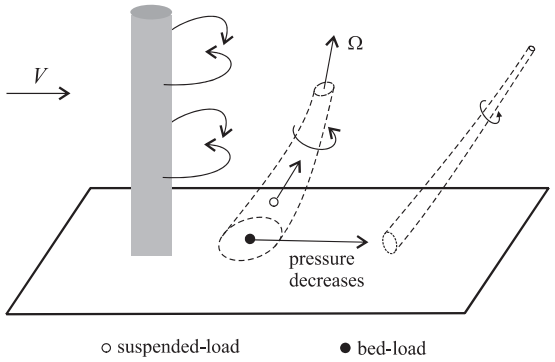

Figure 2 Vortex processes in wake region

in the three directions stretch and tilt the vortex lines so that the fluid particles spin faster (ballerina effect) downstream and upward. Bernoulli's equation states that pressure decreases as velocity increases so that pressure in the wake region decreases downstream and upward. In other words, a favourable pressure gradient forms downstream of the pier and along a vortex line upward (Fig. 2), immediately moving sediment downstream through bed load and suspended load. This is confirmed by Dargahi's (1990) observation: 'the first scour appears in the wake of the cylinder'.

The vertical stagnation flow is qualitatively interpreted by Eq. (17). Bernoulli's equation between the approach flow ($\phi = 0$, $r = \infty$) and the leading pier edge ($\phi = 0, r = R$) states (Fig. 1a)

$$\gamma y + \gamma(h - y) + \frac{1}{2}\rho u^2 = \gamma y + p \tag{23}$$

or

$$p = \gamma(h - y) + \frac{1}{2}\rho u^2 \tag{24}$$

where u, for simplicity, is approximated by the 1/7th power law as

$$u = \frac{8V}{7}\left(\frac{y}{h}\right)^{1/7} \tag{25}$$

with V = approach flow velocity. Inserting Eq. (25) in Eq. (24) gives

$$p = \gamma(h - y) + \frac{32\rho V^2}{49}\left(\frac{y}{h}\right)^{2/7} \tag{26}$$

corresponding to a stagnation point of maximum pressure ($\partial p/\partial y = 0$)

$$\frac{y}{h} = 0.095\mathsf{F}^{2.8} \tag{27}$$

implying that the stagnation point moves upward with increasing F. For $\mathsf{F} = 1$, the stagnation point is at $y/h \approx 10\%$ (1 in Fig. 1a), implying that only a small portion of the stagnation flow becomes the down-flow jet at scour start; a large flow portion turns up, forming the up-flow jet to result in the backwater surface (or bore wave). This value is significantly below the value of Unger and Hager (2007) $y/h \approx 0.8$ for $\mathsf{F} = 0.236$. This difference is

because Eq. (23) neglects the viscous effect and Eq. (25) neglects the pier feedback on the flow field. An improved analysis requires solving stagnation flow from the Reynolds-averaged Navier–Stokes equations or measuring the pressure distribution along the leading edge, which is a future research need.

3.2 *Flow–sediment interaction*

The flow–sediment interaction results from the flow–structure interaction with the pressure gradient determining the sediment movement. If the down-flow impacts the sediment bed, another stagnation point forms where the maximum pressure deflects water upstream of the pier, forming a micro-horseshoe vortex (Fig. 1a). Unger and Hager (2007) observed that such a vortex is usually too weak to initiate scour. Note that this stagnation flow does not turn to the perimeter at scour start because there $\partial p/\partial\phi = 0$ from Eq. (21).

Referring to Fig. 3(a), once scour starts at $\phi = 45°$–$75°$, a domino effect occurs: The favourable pressure gradient along the perimeter pushes the neighbour sediment downstream so that scour increases backward to the stagnation point from both sides. Meanwhile, the favourable pressure gradient due to the tornado-like vortices pushes sediment into the wake region through bed load and suspended load (Fig. 2) to a low-pressure zone (Fig. 3a), where large vortices are diffused into small eddies by viscosity (second term of Eq. 22). A scour ring then results around the pier trapping the micro-horseshoe vortex that is divided into two along the perimeter. A combination of the horseshoe vortex and the favourable pressure gradient in this ring accelerates scour; on the other hand, the combined horseshoe and shedding vortices enhance scour transporting potential in the wake region.

As the scour hole increases, the approach flow velocity profile is redistributed (Fig. 3b) so that the stagnation Point 1 on the leading pier face shifts up (Unger and Hager 2007), the down-flow then becomes stronger, as also the horseshoe vortices, causing a rapid logarithmic scour growth according to Ettema (1980), Dargahi (1989, 1990), and Oliveto and Hager (2002, 2005). Once the stagnation point on the leading pier face shifts to $y/h \approx 0.8$ (Unger and Hager 2007), the down-flow becomes steady. As the scour hole further increases the scour potential is reduced until equilibrium scour is attained, having an inverted-frustum form with the maximum scour depth at the leading pier

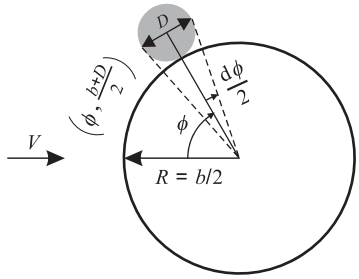

Figure 4 Plan view of sediment–structure interaction: hydrodynamic force on sediment particle

edge. To determine the stagnation Point 1 in Fig. 3(b), accurate approach flow velocity profiles and streamline equations are required, which is beyond this analysis.

3.3 *Sediment–structure interaction*

The sediment–structure interaction is analysed by the hydrodynamic force on individual particles. For a qualitative analysis, it is assumed that (i) the feedback of sediment particles on the flow and the pressure field is negligible and (ii) the qualitative pressure difference between the up- and downstream surfaces is considered.

Referring to Fig. 4, for a sediment particle located at $[\phi, (b + D)/2]$ with $D =$ sediment size in general, the pressure gradient according to Eq. (21) is

$$\frac{\partial p}{\partial \phi} = -\frac{2\rho u^2 \sin 2\phi}{(1 + D/b)^2} \tag{28}$$

From $\mathrm{d}\phi = D/[(b + D)/2]$ in Fig. 4, the approximate pressure difference between the up- and downstream faces is

$$-\frac{\partial p}{\partial \phi}\mathrm{d}\phi = \frac{4\rho u^2 \sin 2\phi}{(1 + D/b)^3}\frac{D}{b} \tag{29}$$

where the negative sign was used because of the favourable pressure gradient. The hydrodynamic force F on the particle is then approximated by

$$F = \left(-\frac{\partial p}{\partial \phi}\mathrm{d}\phi\right)\frac{\pi D^2}{4} = \frac{\pi\rho u^2 D^2 \sin 2\phi}{(1 + D/b)^3}\frac{D}{b} \tag{30}$$

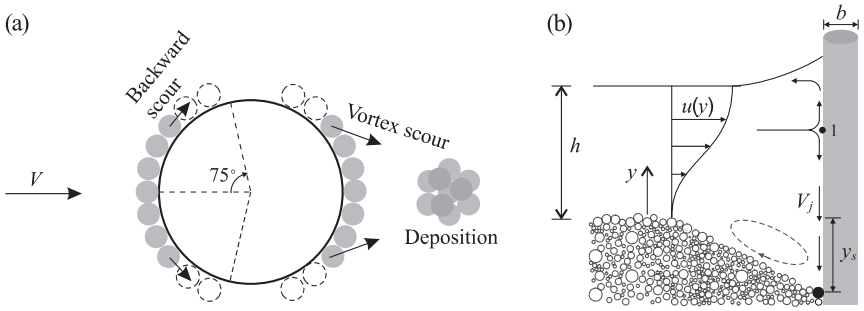

Figure 3 Flow–sediment interaction: (a) plane view of the initial phase and (b) side view of the equilibrium phase

Considering that the submerged sediment weight $W = (\rho_s - \rho)g(\pi D^3/6)$ resists scour in the flow–sediment interaction, the local scour potential depends on

$$\frac{F}{W} \propto \frac{\rho u^2}{(\rho_s - \rho)gb} \frac{\sin 2\phi}{(1 + D/b)^3} \propto \frac{V^2}{(\rho_s/\rho - 1)gb} \frac{\sin 2\phi}{(1 + D/b)^3} \tag{31}$$

where $u \propto V$ was used and D/b represents the sediment–structure interaction. The local scour mainly depends on the flow–structure interaction $V/(gb)^{1/2}$, while the sediment–structure interaction D/b can be neglected due to $D/b \ll 1$ in practice, as was indicated by Melville and Chiew (1999). Both $V/(gb)^{1/2}$ and D/b do not affect y_s at $\phi = 0$ so that Eq. (16) is reduced to

$$\frac{y_s}{b^\lambda h^{1-\lambda}} = \mathrm{f}(\mathsf{H}, \sigma) \tag{32}$$

which does not support f_3 in Eq. (10). Note that the effect of D/b needs further research because Eq. (32) is drawn from Eq. (31) or from Eq. (21) at scour start instead of the equilibrium stage.

This section is summarized as: (i) along the pier perimeter, the flow–structure interaction results in a favourable pressure gradient transporting sediment (flow–sediment interaction) to the wake region; (ii) the vortex processes in the wake region result in a favourable pressure gradient downstream and upward, moving sediment further downstream; (iii) the down-flow from the flow–structure interaction generates horseshoe vortices to scour and move sediment downstream; and (iv) the equilibrium scour depth from Eq. (32) at the leading pier edge is determined by the flow–structure and flow–sediment interactions, independent of the sediment–structure interaction. Equation (32) is further detailed below.

4 Hypothesis: equilibrium scour depth

The scour mechanism previously described includes the complicated processes of flow-structure-sediment interactions. If only the equilibrium scour depth at the leading edge (Fig. 3b) is considered, then the problem is simplified. The flow first impacts a pier at the leading face generating a down-flow resulting in a scour hole. The larger the pier blockage area, the stronger is the down-flow, so that the scour hole becomes deeper. Therefore, the scour depth y_s increases with the blockage area as

$$y_s \propto (bh)^\alpha \tag{33}$$

with $\alpha > 0$. Equation (33) implies that $y_s = 0$ if $bh = 0$, which is physically reasonable.

Referring to Fig. 5, the down-flow of velocity V_j generates a lateral hydrodynamic force $F_l \propto \rho V_j^2 D_j^2$ to the sediment D_j below the jet. This force, similar to a lift, results from the pressure over the asymmetrical natural sediment surface transporting the sediment, while the submerged sediment weight W resists scour through friction, $F_f \propto W$. Therefore, the scour potential at the

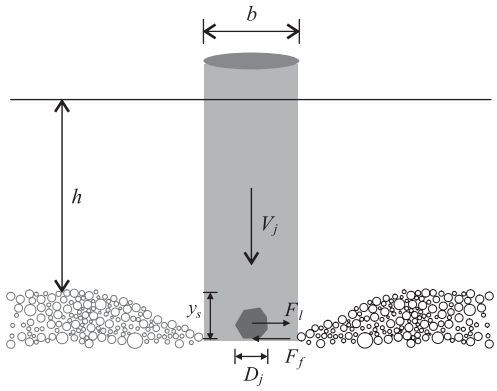

Figure 5 Upstream view of equilibrium scour hole

maximum scour depth depends on the relative strength between F_l and F_f

$$\frac{F_l}{F_f} \propto \frac{F_l}{W} \propto \frac{\rho V_j^2 D_j^2}{(\rho_s - \rho)gD_j^3} \propto \frac{V^2}{(\rho_s/\rho - 1)gD_j} \tag{34}$$

where $V_j \propto V$ was used. Note that Eqs. (34) and (31) result from two different mechanisms. Experiments (Richardson and Davis 2001) indicate that $D_j \cong D_{90}$ for sediment mixtures. For simplicity, this research assumes $D_j = D_{50}\sigma^{3/2}$, corresponding to D_{93} if sediment sizes obey the log-normal distribution. Equation (34) then becomes

$$\frac{F_l}{F_f} \propto \frac{V^2}{(\rho_s/\rho - 1)gD_{50}\sigma^{3/2}} = \frac{\mathsf{H}^2}{\sigma^{3/2}} \tag{35}$$

implying that

$$y_s \propto \mathrm{f}\left(\frac{\mathsf{H}^2}{\sigma^{3/2}}\right) \tag{36}$$

Combining Eqs. (33) and (36) gives

$$y_s = (bh)^\alpha \mathrm{f}\left(\frac{\mathsf{H}^2}{\sigma^{3/2}}\right) \tag{37}$$

with $\alpha = 1/2$ according to dimensional homogeneity. Equation (37) is then rewritten as

$$\frac{y_s}{\sqrt{bh}} = \mathrm{f}\left(\frac{\mathsf{H}^2}{\sigma^{3/2}}\right) \tag{38}$$

stating that (i) $(bh)^{1/2}$ is the scaling length for y_s, consistent with Eq. (16) or (32) where $\lambda = 1/2$ and (ii) the dimensionless scour depth $y_s/(bh)^{1/2}$ is determined by the Hager number H and sediment non-uniformity σ, similar to Eq. (9). Below Eq. (38) is tested and its specific functional form is determined.

5 Test of hypothesis

Equation (38) is tested using the CSU data (Molinas 2001) collected from three flumes including 10 tests with various V, h, b, D_{50} and σ. The test conditions are summarized in Table 1.

In total, 171 tests were conducted while only 82 are used here, selected by the criteria: (i) approach average velocity $V < V_c$ (Richardson and Davis 2001) at the sediment threshold for D_{50} so that the bed upstream of the pier is not significantly scoured ensuring that the approach flow conditions are not significantly changed, resulting in clear-water condition; (ii) flow depth is limited to $1 \leq h/b \leq 6$, ensuring that y_s is not affected by the bore wave from the up-flow and the vertical stagnation point depends on h so that the hypothesis of Eq. (33) is valid; (iii) only tests with natural sediment mixtures were used, with the sediment sizes approximated by the log-normal distribution; tests with artificial sediment mixtures were excluded so that the hypothesis of Eq. (35) is valid. Note that equilibrium scour conditions need a long duration for uniform sediment, yet the runs considered reached their equilibrium states because of the armouring effect of sediment mixtures.

The selected data with three D_{50} and four σ are plotted in Fig. 6 according to Eq. (38). Note that most data fall into a narrow strip, so that Eq. (38) is reasonable but imperfect. The scatter of data results from the fact that a universal critical value of $\mathsf{H}^2/\sigma^{3/2}$ does not exist for pier scour inception but varies with the flow–structure–sediment conditions (Hager and Oliveto 2002). Like Eq. (11), the data in Fig. 6 can be approximated by a hyperbolic tangent as

$$\frac{y_s}{\sqrt{bh}} = \tanh\left(\frac{\mathsf{H}^2/\sigma^{3/2} - \mathsf{H}_{cp}^2}{3.75}\right) \tag{39}$$

Table 1 Summary of test conditions for CSU data

Flumes	Hydrodynamics flume: 0.6 m wide, 0.75 m deep, 18 m long
	Sedimentation flume: 2.4 m wide, 1.2 m deep, 60 m long
	River mechanics flume: 6 m wide, 0.9 m deep, 30 m long
Measurements	Discharge by orifice plates to 3–5%
	Velocity by electronic velocity meters to 2–5%
	Flow and scour depth by point gauge to ± 1.5 mm
	Sediment size distribution by sieve analysis
Flow conditions	$V = 0.15$–2.5 m/s, $h = 0.04$–0.38 m, test duration = 8–20 h
Structures	$b = 0.019$–0.216 m, pier-to-width ratio $\leq 7\%$
Sediment mixtures	$D_{16} = 0.22$–13.0 mm, $D_{35} = 0.40$–16.1 mm, $D_{50} = 0.55$–16.9 mm
	$D_{84} = 1.03$–20.2 mm, $D_{95} = 1.08$–42.4 mm, $D_{99} = 1.19$–45.0 mm
	$\sigma = 1.15$–3.70

Note: Artificial coarse sands were added to natural size distributions in some tests.

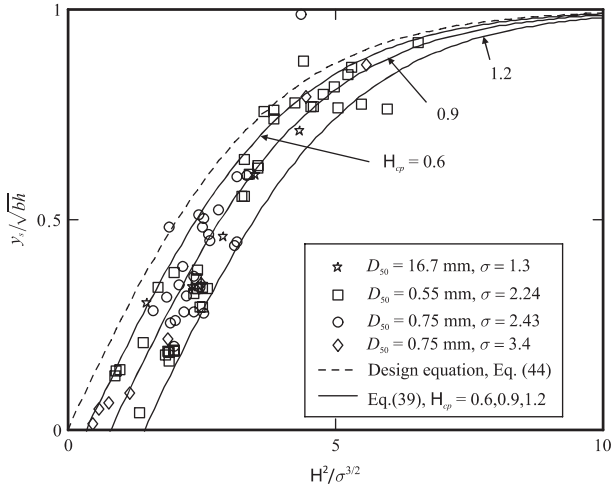

Figure 6 Test of scour hypothesis with CSU data

where H_{cp} = critical Hager number for $\sigma = 1$. The solid lines in Fig. 6 correspond to $\mathsf{H}_{cp} = 0.6$, 0.9 and 1.2 with 0.6 as the upper envelope. According to Hager and Oliveto (2002),

$$\mathsf{H}_{cp} = \left[1 - \frac{2}{3}\left(\frac{b}{B}\right)^{1/4}\right]\mathsf{H}_c \tag{40}$$

where B = channel width and H_c = critical Hager number corresponding to

$$\mathsf{H}_c = \begin{cases} 2.33 D_*^{-0.25}\left(\dfrac{R_h}{D_{50}}\right)^{1/6} & \text{for } D_* \leq 10 \\ 1.08 D_*^{1/12}\left(\dfrac{R_h}{D_{50}}\right)^{1/6} & \text{for } 10 < D_* < 150 \\ 1.65\left(\dfrac{R_h}{D_{50}}\right)^{1/6} & \text{for } D_* \geq 150 \end{cases} \tag{41}$$

where $D_* = [(\rho_s/\rho - 1)g/v^2]^{1/3} D_{50}$ = dimensionless sediment size, and R_h = hydraulic radius.

For small H or weak scour, Eq. (39) is approximated by

$$\frac{y_s}{\sqrt{bh}} = \frac{\mathsf{H}^2/\sigma^{3/2} - \mathsf{H}_{cp}^2}{3.75} \tag{42}$$

indicating that $y_s \propto \mathsf{H}^2$ if H_{cp} is neglected, or $y_s \propto V^2$, in agreement with Oliveto and Hager (2002): 'the scour depth increases with the approach flow velocity, approximately following the square relation'. For large H or strong scour, Eq. (39) tends to

$$\frac{y_s}{\sqrt{bh}} = 1 \tag{43}$$

corresponding to the maximum potential scour depth, similar to Eq. (3) or (6) for intermediate piers. Briefly, Eq. (38) is confirmed with the CSU data, but a critical Hager number needs to be considered for accurate scour predictions; y_s is approximated by a hyperbolic tangent as given in Eq. (39), with a maximum potential scour depth of $y_s = (bh)^{1/2}$.

6 Applications in foundation design and scour evaluation

The proposed Eq. (39) applies for bridge foundation design and scour evaluation as important items in bridge construction and maintenance. Given the flow–structure–sediment conditions, Eqs. (39)–(41) provide a design basis for equilibrium scour depth y_s. To eliminate uncertainties in estimating H_{cp}, a conservative design is proposed by dropping H_{cp} from Eq. (39)

$$\frac{y_s}{\sqrt{bh}} = \tanh\left(\frac{\mathsf{H}^2/\sigma^{3/2}}{3.75}\right) \tag{44}$$

plotted in Fig. 6 as a dashed line, indicating that the design depth based on Eq. (44) is statistically larger than real scour depths. Furthermore, Eq. (43) gives a rule of thumb for the foundation design. Consider, for example, a circular pier of $b = 0.5$ m in a river with a 100-year flood at depth $h = 3$ m, the maximum potential scour depth is $y_s = 1.22$ m.

Equation (43) is compared with Eqs. (3) and (11) in Fig. 7, showing that the proposed design equation gives the lowest y_s for $h/b \leq 6$, while for $h/b > 6$ Sheppard–Melville's equation gives the lowest value of 2.5 corresponding to the maximum potential value in observations (Ettema *et al.* 2011). Therefore, this research recommends Eq. (43) for design purposes if $h/b \leq 6$ and Eq. (11) or (13) if $h/b > 6$ (deep water). Of course, the correction factors in Eq. (4) may be considered in practice except for K_4 due to sediment mixtures. During floods, bridge managers could estimate scour conditions at critical moments and formulate timely corrective strategies according to Eqs. (43) and (44). A bridge is safe if the estimated scour depth y_s is less than the foundation depth. Otherwise, conditions are critical and the bridge should be closed for public safety; the damage should be immediately repaired after floods.

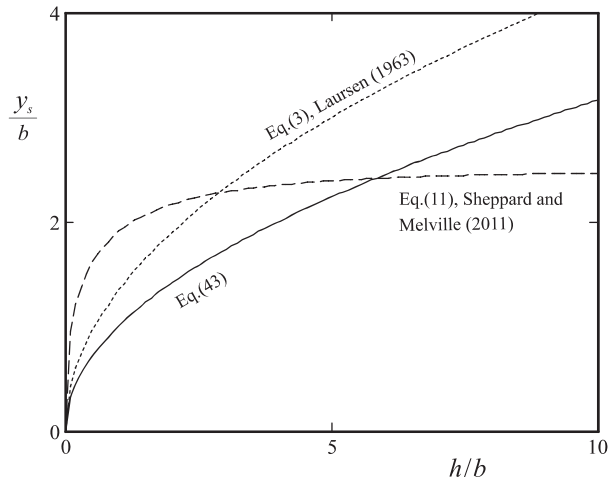

Figure 7 Comparison of various design equations for maximum potential scour design

7 Further research needs

This research can be improved if the following researches are pursued in the future.

- Equation (38) states that y_s is scaled by $(bh)^{0.5}$, corresponding only to the intermediate pier of Eq. (6). An experimental study is then needed to determine the extremes of Eq. (38) by studying the vertical stagnation flow at the leading pier face.
- It is usually assumed that $y_s \neq \mathrm{f}(h)$ for deep-water scour without data support because most of the available tests were run in flumes of limited flow depths. To eliminate the h effect, a wind tunnel experiment would identify the vertical stagnation point at the leading pier face.
- This research excludes the effect of D/b in Eq. (32) based on the flow analysis at scour start instead of the equilibrium stage. Therefore, numerical and experimental researches are needed on the sediment–structure interaction under equilibrium flow conditions.

8 Conclusions

After a critical review of pier scour in clear water for sediment mixtures, the relevant scour mechanism and a scour depth equation were proposed to understand the pier scour processes and the scour design. In general, pier scour results from flow–structure–sediment interactions, and the equilibrium scour depth is determined by the flow–structure and the flow–sediment interactions. The following conclusions are drawn.

(1) The flow–structure interaction sets up a favourable pressure gradient along the pier perimeter and in the wake region. The perimeter pressure gradient is explained by the classic boundary layer theory; the wake pressure gradient by the conservation of vorticity. The flow–structure interaction also results in a vertical stagnation flow, generating horseshoe vortices at the foot of the pier playing an important role in the formation of maximum equilibrium scour depth.

(2) The flow–sediment interaction results from the flow–structure interaction where the pressure gradient determines sediment motion. The favourable perimeter pressure gradient and the horseshoe vortices thus dislodge sediment to the wake of pier; the wake-favourable pressure gradient due to vortex motion further moves sediment downstream to a low-pressure zone where large vortices are broken into small eddies.

(3) The sediment–structure interaction has a small effect on the scour processes and the equilibrium scour depth at the leading edge.

(4) The equilibrium scour depth is hypothesized to increase with the pier blockage area and the Hager number, but decreases with sediment non-uniformity. This hypothesis was confirmed by the CSU data with various flow–structure–sediment conditions.

(5) The proposed results apply for scour design and evaluation. A rule of thumb is that the maximum potential scour depth is equal to the square root of the product of the pier diameter and the approach flow depth.
(6) This research is based on a limited database, indicating that extensive experimental research and further analyses are needed for a complete understanding of pier scour in clear water for sediment mixtures.

Acknowledgements

This research was supported by the US Federal Highway Administration Hydraulics R&D Program with Contract No. DTFH61-11-D-00010 through the Genex System to the University of Nebraska-Lincoln. The author thanks the visiting student Mr Oscar Berrios for the data preparation.

Notation

B = channel width (m)
b = pier diameter (m)
D = sediment size in general (m)
$\mathrm{D}/\mathrm{D}t$ = material derivative (s^{-1})
D_* = dimensionless sediment size ($^-$)
D_i = sediment size finer than i% of sediment (m)
D_j = sediment size just under down-flow (m)
D_{50} = median sediment size (m)
F = approach flow Froude number (–)
F = hydrodynamic force (N)
F_f = frictional force (N)
F_l = lateral hydrodynamic force (N)
f, f_i = functional symbol $i = 1, 2, 3$ (–)
g = gravitational acceleration (m/s^2)
H = Hager number (–)
H_c = critical value of H (–)
H_{cp} = critical value of H corresponding to pier scour (–)
h = approach flow depth (m)
K_i = correction factor $i = 1, 2, 3, 4(-)$
p = pressure (N/m^2)
R = pier radius $R = b/2$ (m)
R_h = hydraulic radius (m)
r = distance from pier centre (m)
t = time (s)
$\mathbf{u}$ = vector velocity (m/s)
u = velocity distribution (m/s)
u_r = potential velocity in radial direction (m/s)
u_ϕ = potential velocity along the perimeter (m/s)
V = approach average flow velocity (m/s)
V_c = approach critical velocity at sediment threshold (m/s)
W = submerged weight of sediment (N)
y = distance from bed (m)
y_s = equilibrium scour depth (m)
α = exponent (−)
γ = specific water weight (N/m^3)
λ = exponent (−)
ν = kinematic water viscosity (m^2/s)
ρ = water density (kg/m^3)
ρ_s = sediment density (kg/m^3)
σ = sediment non-uniformity $\sigma = (D_{84}/D_{16})^{1/2}$ (−)
τ_c = critical shear stress at sediment threshold (N/m^2)
τ_1 = grain component of bed-shear stress (N/m^2)
ϕ = angle (−)
$\mathbf{\Omega}$ = vorticity (s^{-1})

References

Abdelaziz, S., Bui, M.D., Rutschmann, P. (2011). Numerical investigation of flow and sediment transport around a circular bridge pier. Proc. 34th *IAHR World Congress* Brisbane, 3296–3304.

Dargahi, B. (1989). The turbulent flow field around a circular cylinder. *Exp. Fluids* 8(1–2), 1–12.

Dargahi, B. (1990). Controlling mechanism of local scouring. *J. Hydraulic Eng.* 116(10), 1197–1214.

Dey, S., Raikar, R.V. (2007). Characteristics of horseshoe vortex in developing scour holes at piers. *J. Hydraulic Eng.* 133(4), 399–413.

Einstein, H.A., El-Samni, E.S.A. (1949). Hydrodynamic forces on a rough wall. *Rev. Mod. Phys.* 21(3), 520–524.

Ettema, R. (1980). Scour at bridge piers. *Report* No. 216. School of Eng., Univ. of Auckland, Auckland, NZ.

Ettema, R., Constantinescu, G., Melville, B. (2011). *Evaluation of bridge scour research: Pier scour processes and predictions*. NCHRP Web-Only Document 175. Transportation Research Board of the National Academies, Washington, DC.

Hager, W.H., Oliveto, G. (2002). Shields' entrainment criterion in bridge hydraulics. *J. Hydraulic Eng.* 128(5), 538–542.

Hager, W.H., Unger, J. (2010). Bridge pier scour under flood waves. *J. Hydraulic Eng.* 136(10), 842–847.

Hjorth, P. (1975). *Studies on the nature of local scour*. Bull. Ser. A, No. 46. Dept. of Water Resources Eng., Univ. of Lund, Sweden.

Inglis, S.C. (1949). *Maximum depth of scour at heads of guide bands and groynes, pier noses, and downstream bridges-the behavior and control of rivers and canals*. Indian Waterways Experimental Station, Poona, India.

Julien, P.Y. (2010). *Erosion and sedimentation*, 2nd ed. Cambridge Univ. Press, New York.

Kandasamy, J.K., Melville, B.W. (1998). Maximum local scour depth at bridge piers and abutments. *J. Hydraulic Res.* 36(2), 183–198.

Kirkil, G., Constantinescu, S.G., Ettema, R. (2008). Coherent structures in the flow field around a circular cylinder with scour hole. *J. Hydraulic Eng.* 134(5), 572–587.

Kirkil, G., Constantinescu, S.G., Ettema, R. (2009). Detached eddy simulation investigation of turbulence at a circular pier with scour hole. *J. Hydraulic Eng.* 135(11), 888–901.

Kothyari, U.C., Hager, W.H., Oliveto, G. (2007). Generalized approach for clear-water scour at bridge foundation elements. *J. Hydraulic Eng.* 133(11), 1229–1240.

Kundu, P.K. (1990). *Fluid mechanics*. Academic Press, Burlington, MA.

Laursen, E.M. (1958). Scour at bridge crossings. *Bulletin* No.8. Iowa Highway Research Board, Ames, IA.

Laursen, E.M. (1963). An analysis of relief bridge scour. *J. Hydraulics Div.* ASCE 89(HY3), 93–118.

Melville, B.W. (1997). Pier and abutment scour: integrated approach. *J. Hydraulic Eng.* 123(2), 125–136.

Melville, B.W., Chiew, Y.-M. (1999). Time scale for local scour at bridge piers. *J. Hydraulic Eng.* 125(1), 59–65.

Molinas, A. (2001). *Effects of gradation and cohesion on bridge scour*: Synthesis report. FHWA-RD-99-189. Federal Highway Administration, Washington, DC.

Oliveto, G., Hager, W.H. (2002). Temporal evolution of clear-water pier and abutment scour. *J. Hydraulic Eng.* 128(9), 811–820.

Oliveto, G., Hager, W.H. (2005). Further results to time-dependent local scour at bridge elements. *J. Hydraulic Eng.* 131(2), 97–105.

Richardson, E.V., Davis, S.R. (1995). *Evaluating scour at bridges*, 3rd ed. *Hydraulic Engineering Circular* No. 18, FHWA IP-90-017. Federal Highway Administration, Washington, DC.

Richardson, E.V., Davis, S.R. (2001). *Evaluating scour at bridges*, 4th ed. *Hydraulic Engineering Circular* No. 18, FHWA NHI 01-001. Federal Highway Administration, Washington, DC.

Roulund, A., Sumer, B.M., Fredsøe, J., Michelsen, J. (2005). Numerical and experimental investigation of flow and scour around a circular pile. *J. Fluid Mech.* 534, 351–401.

Shen, H.W., Schneider, V.R., Karaki, S.S. (1966). *Mechanics of local scour*. Civil Engineering Department, Engineering Research Center, Colorado State University, Ft. Collins CO.

Sheppard, D.M, Demir, H., Melville, B.W. (2011). *Scour at wide piers and long skewed piers*. NCHRP Report 682, Transportation Res. Board of National Academies, Washington, DC.

Sheppard, D.M., Miller, W., Jr. (2006). Live-bed local pier scour experiments. *J. Hydraulic Eng.* 132(7), 635–642.

Shirole, A.M., Holt, R.C. (1991). Planning for comprehensive bridge safety assurance program. *Transp. Res. Rec*. 1290, 39–50.

Sumer, B.M. (2007). Mathematical modelling of scour: A review. *J. Hydraulic Res.* 45(6), 723–735.

Tafarojnoruz, A., Gaudio, R., Dey, S. (2010). Flow-altering countermeasures against scour at bridge piers: A review. *J. Hydraulic Res.* 48(4), 441–452.

Unger, J., Hager, W.H. (2007). Down-flow and horseshoe vortex characteristics of sediment embedded bridge piers. *Exp. Fluids* 42(1), 1–19.

Veerappadevaru, G., Gangadharaiah, T., Jagadeesh, T.R. (2011). Vortex scouring process around bridge pier with a caisson. *J. Hydraulic Res.* 49(3), 378–383.

White, F.M. (1991). *Viscous fluid flow*, 2nd ed. McGraw-Hill, New York.